# Durham Research Online

# No cores in dark matter-dominated dwarf galaxies with bursty star formation histories

Sownak Bose[1]*, Carlos S. Frenk[2], Adrian Jenkins[2], Azadeh Fattahi[2],
Facundo A. Gómez[3,4], Robert J. J. Grand[5,6], Federico Marinacci[1],
Julio F. Navarro[7], Kyle A. Oman[8,7], Rüdiger Pakmor[9], Joop Schaye[10],
Christine M. Simpson[11,12,5], and Volker Springel[9,5,6]

[1] *Harvard-Smithsonian Center for Astrophysics, 60 Garden St., Cambridge, MA 02138, USA*
[2] *Institute for Computational Cosmology, Durham University, South Road, Durham, DH1 3LE, UK*
[3] *Instituto de Investigación Multidisciplinar en Ciencia y Tecnología, Universidad de La Serena, Raúl Bitrán 1305, La Serena, Chile*
[4] *Departamento de Física y Astronomía, Universidad de LaSerena, Av. Juan Cisternas 1200 N, La Serena, Chile*
[5] *Heidelberger Institut für Theoretische Studien, Schloß-Wolfsbrunnenweg 35, 69118 Heidelberg, Germany*
[6] *Zentrum für Astronomie der Universität Heidelberg, Astronomisches Recheninstitut, Mönchhofstr. 12-14, 69120 Heidelberg, Germany*
[7] *Department of Physics and Astronomy, University of Victoria, PO Box 3055 STN CSC, Victoria, BC, V8W 3P6, Canada*
[8] *Kapteyn Astronomical Institute, University of Groningen, Postbus 800, NL-9700 AV Groningen, The Netherlands*
[9] *Max-Planck-Institut für Astrophysik, Karl-Schwarzschild-Str. 1, D-85748, Garching, Germany*
[10] *Leiden Observatory, Leiden University, PO Box 9513, 2300 RA Leiden, The Netherlands*
[11] *Enrico Fermi Institute, The University of Chicago, Chicago, IL 60637, USA*
[12] *Department of Astronomy & Astrophysics, University of Chicago, Chicago, IL 60637, USA*

26 April 2019

**ABSTRACT**

Measurements of the rotation curves of dwarf galaxies are often interpreted as requiring a constant density core at the centre, at odds with the "cuspy" inner profiles predicted by $N$-body simulations of cold dark matter (CDM) haloes. It has been suggested that this conflict could be resolved by fluctuations in the inner gravitational potential caused by the periodic removal of gas following bursts of star formation. Earlier work has suggested that core formation requires a bursty and extended star formation history (SFH). Here we investigate the structure of CDM haloes of dwarf galaxies ($M_{\rm DM} \sim 10^9 - 5 \times 10^{10}\,{\rm M_\odot}$) formed in the APOSTLE ('A Project of Simulating the Local Environment') and AURIGA cosmological hydrodynamic simulations. Our simulations have comparable or better resolution than others that make cores ($M_{\rm gas} \sim 10^4\,{\rm M_\odot}$, gravitational softening $\sim 150$ pc). Yet, we do not find evidence of core formation at *any* mass or any correlation between the inner slope of the DM density profile and temporal variations in the SFH. APOSTLE and AURIGA dwarfs display a similar diversity in their cumulative SFHs to available data for Local Group dwarfs. Dwarfs in both simulations are DM-dominated on all resolved scales at all times, likely limiting the ability of gas outflows to alter significantly the central density profiles of their haloes. We conclude that recurrent bursts of star formation are not sufficient to cause the formation of cores, and that other conditions must also be met for baryons to be able to modify the central DM cusp.

**Key words:** cosmology: dark matter – galaxies: dwarf – galaxies: haloes – galaxies: Local Group – galaxies: star formation

## 1 INTRODUCTION

The existence of dark matter (DM) in the form of cold, collisionless particles is the bedrock of the currently favoured model of cosmology, ΛCDM. In this model, the accelerated expansion of the Universe on large scales is dominated by vacuum energy in the form of a cosmological constant, Λ, while structure formation on

small scales proceeds hierarchically through the gravitational collapse of cold dark matter (CDM) particles into DM "haloes". The theory of galaxy formation, which has matured over the last four decades, has painted a picture where baryons are able to cool and condense into these DM haloes, eventually forming the stars that make up a galaxy (White & Frenk 1991). The death of massive stars in the form of supernovae releases energy back into the surrounding gas, reheating it to suppress further star formation, before radiative cooling of this heated gas is able to kick-start star forma-

* Email: sownak.bose@cfa.harvard.edu

tion once again (e.g. Larson 1974; Dekel & Silk 1986; Katz et al. 1996; Somerville & Primack 1999; Cole et al. 2000).

A feature of the CDM model that has enhanced its prominence is that it is highly predictive. Many of its predictions, particularly in the non-linear regime of structure formation, have come from an intensive programme of $N$-body simulations over the past three decades (see Frenk & White 2012, for a recent review). A fundamental prediction from collisionless $N$-body simulations is that DM haloes develop density profiles with steeply rising slopes in the inner part of the halo, described by the Navarro-Frenk-White (NFW) density profile (Navarro et al. 1996b, 1997). This profile rises as $\rho \propto r^{-1}$ in the centre, resulting in a central "cusp", as $\rho \propto r^{-3}$ in the outer parts, and as $\rho \propto r^{-2}$ in between. The NFW profile is universal (i.e. independent of halo mass, but see e.g. Anderhalden & Diemand 2013; Ishiyama 2014; Angulo et al. 2017, for claimed deviations at much smaller mass scales).

In conjunction with simulations, our understanding of the Universe around us has also been augmented by the exquisite observational data now available, especially for galaxies in the Local Group. DM-dominated dwarf galaxies, in particular, are ideal for investigating the interplay between the gravitational collapse of DM and the physics of galaxy formation. These investigations, however, have not been without controversy. It has been claimed that the DM density profiles of dwarf galaxies, inferred from their H I rotation curves or stellar kinematics, reveal the presence of a near constant density inner "core", in stark contrast with the prediction of the NFW model (Moore 1994; Flores & Primack 1994; Burkert 1995; de Blok et al. 2001; Kuzio de Naray & Kaufmann 2011; Hague & Wilkinson 2013; Oh et al. 2015). This mismatch between theory and observation, the so-called *core-cusp problem*, is often cited as one of the greatest challenges faced by the CDM paradigm.

In reply, theorists have proposed mechanisms to induce cores in originally cuspy profiles. The main idea goes back to the work of Navarro et al. (1996a) who showed that a core can be produced by the sudden removal of gas (by energy injected from supernovae) from the centre of a cuspy halo in which gas had previously cooled gradually until dominating the gravitational potential. To illustrate this mechanism they assumed an initial analytic mass distribution corresponding to a cuspy density profile[1] which was perturbed by the potential of a gradually growing baryonic disk. To mimic the effect of an energetic outflow, the disk potential was removed abruptly; the DM responds to this change by settling into a new equilibrium configuration with a central core whose size depends on the strength of the perturbation.

The idea that energetic outflows may generate cores was further developed by Read & Gilmore (2005) and Mashchenko et al. (2006, 2008) who argued that a *series* of localised, moderately violent outbursts, is a more efficient way of generating a core than the single, explosive outburst mechanism of Navarro et al. (1996a). The process was first seen in cosmological hydrodynamic simulations by Governato et al. (2010) and Parry et al. (2012), and the physics behind core creation through repeated outbursts was later detailed by Pontzen & Governato (2012). Their proposed model describes oscillations in the gas potential generated by repeated bursts that eventually transfer energy to the DM, expanding the orbits of particles near the halo centre, transforming a cusp into a core. Governato et al. (2010) also found that the efficacy of this

mechanism depends on the threshold density for star formation, $n_{\rm sf}$, assumed in the simulation. A low threshold ($n_{\rm sf} = 0.1$ cm$^{-3}$) preserves a cusp, while a high threshold ($n_{\rm sf} = 100$ cm$^{-3}$) leads to a core. More recently, El-Zant et al. (2016) have proposed a theoretical framework for understanding the mechanisms for core formation in terms of statistical properties of fluctuations in the gaseous component of the halo.

Several hydrodynamical simulations have reported a connection between the formation of cores and the star forming efficiency of dwarf galaxies. For example, Di Cintio et al. (2014); Tollet et al. (2016) and Macciò et al. (2017) find a strong dependence of the inner slope of the DM density profile on the final stellar-to-halo mass ratio, $M_\star/M_{\rm h}$. Galaxies in which star formation is inefficient ($M_\star/M_{\rm h} \lesssim 10^{-4}$), do not form cores; conversely, highly star forming galaxies ($M_\star/M_{\rm h} \gtrsim 10^{-2}$) develop even cuspier profiles than their DM-only counterparts due to adiabatic contraction (e.g. Duffy et al. 2010; Schaller et al. 2015a). These limits bracket a "sweet-spot" for core creation at $M_\star/M_{\rm h} \sim 10^{-2}$. An interesting result of these works is that the *qualitative* relationship between the inner slope of the profile and $M_\star/M_{\rm h}$ is seemingly independent of the specific feedback implementation in the simulations.

Using the FIRE simulations (Hopkins et al. 2014, 2018), Oñorbe et al. (2015) and Chan et al. (2015) found that while all their simulated dwarfs exhibited extremely bursty SFRs (i.e. showing $\sim$ order of magnitude fluctuations in the SFR over a dynamical time), the ones that preferentially formed cores were those with a substantial amount of late-time star formation (a similar observation has also been made more recently by Read et al. 2018). This stems primarily from the fact that haloes that form cores during early bursts of star formation are subject to many subsequent events of mass accumulation through mergers and smooth accretion (during what is known as the 'rapid accretion phase'; see e.g. Wechsler et al. 2002). The result of this is that 'transient' cores are formed, which eventually reassemble into cusps through these accretion events (e.g. Laporte & Peñarrubia 2015). The requirements for core formation were refined further by Fitts et al. (2017), who corroborated the limit of $\sim 10^6 {\rm M}_\odot$ as the 'threshold' stellar mass needed to form cores in dwarf galaxy haloes as previously reported by e.g. Madau et al. (2014). In other words, these authors find that dwarf galaxies that exhibit the highest *star formation efficiency* have the greatest propensity to form cores.

Other authors have proposed more exotic alternatives to CDM in which the dynamics of the particles lead naturally to core formation on the mass scales of interest. The most popular amongst these is warm dark matter (WDM, Bond & Szalay 1983; Colín et al. 2000; Bode et al. 2001). The free-streaming of WDM particles suppresses density fluctuations below a characteristic mass scale imposing constraints on the available phase-space for the DM particles that result in the formation of a core. However, Villaescusa-Navarro & Dalal (2011) and Shao et al. (2013) have shown that for WDM models that are observationally viable, the cores are too small to be astronomically interesting, a result seen in recent cosmological simulations where the overall NFW shape is preserved on the scales of interest (see, e.g. Lovell et al. 2014; Bose et al. 2016; Bozek et al. 2016). A more promising alternative are self-interacting DM models, where multiple scattering events between DM particles can result in the formation of constant density cores by removing particles from the centres of haloes (e.g. Vogelsberger et al. 2012; Zavala et al. 2013; Rocha et al. 2013; Robertson et al. 2018).

Our objective in this paper is to examine the link, if any, between the shape of the DM density profiles of dwarf galaxy haloes

---

[1] Navarro et al. (1996a) used the cuspy Hernquist profile (Hernquist 1990) to represent the DM density distribution.

and their SFHs in cosmological, hydrodynamical simulations of Milky Way and Local Group-like environments. We investigate dwarf galaxies extracted from the APOSTLE (Fattahi et al. 2016b; Sawala et al. 2016) and AURIGA (Grand et al. 2017) projects. An important feature of the galaxy formation models implemented in these simulations is that very similar subgrid prescriptions have been shown to reproduce a wide variety of properties of the galaxy population as a whole, such as the stellar mass function of galaxies, the bimodality of their colour distributions, etc. (e.g. Schaye et al. 2015; Trayford et al. 2017; Pillepich et al. 2018b; Nelson et al. 2018). This point, and more specific details of these simulations, are elaborated on in Section 2.

This paper is organised as follows. In Section 2, we introduce the simulations used in this work and outline the criteria to select an appropriate sample of dwarf galaxies (Section 2.3). Section 3 presents our main results: the DM density profiles of dwarf galaxy haloes and the evolution of these profiles in time (Section 3.1); the bursty star formation rates of our simulated dwarfs and the SFHs of our sample compared with observational data (Section 3.4). In Section 4, we discuss possible reasons why our simulations do not form cores at any mass. Finally, our conclusions are summarised in Section 5.

## 2 SIMULATIONS

In this section, we provide brief descriptions of APOSTLE and AU-RIGA, which are the sets of hydrodynamical simulations analysed in this paper.

### 2.1 The APOSTLE simulations

The APOSTLE ('A Project Of Simulating The Local Environment') simulation suite consists of a set of zoom-in hydrodynamical simulations representing analogues of the Local Group and its environment (Fattahi et al. 2016b; Sawala et al. 2016). Pairs of haloes with total mass, separation, and relative radial and tangential velocities consistent with the Milky Way-M31 pair were selected from a periodic, cosmologically representative dark matter only (DMO) simulation with a comoving box size of 100 Mpc. The selected regions were then re-simulated at higher resolution. The cosmological parameters used in both the parent volume and each of the APOS-TLE re-simulations are consistent with WMAP-7 (Komatsu et al. 2011): $\Omega_m = 0.272$, $\Omega_b = 0.0455$, $\Omega_\Lambda = 0.728$ and $h = 0.704$, where $h$ is related to the present day Hubble constant, $H_0$, by $h = H_0/100\,\mathrm{kms}^{-1}\mathrm{Mpc}^{-1}$. The spectral index of the primordial power spectrum, $n_s = 0.967$; the linear power spectrum is normalised at $z = 0$ using $\sigma_8 = 0.81$.

In total, 12 regions were selected for re-simulation as part of the APOSTLE simulation suite. While all 12 volumes were re-simulated at 'low' and 'medium' resolution (L3 and L2), six APOS-TLE volumes have also been run at 'high' resolution (L1), three of which are used in the present analysis (which we will label 'Ap-V1', 'Ap-V4' and 'Ap-V6' in the rest of this paper). In the APOS-TLE L1 simulations, a single dark matter particle has a mass of $m_{\mathrm{DM}} \sim 4 \times 10^4 \mathrm{M}_\odot$, a single gas particle initially has an average mass of $m_{\mathrm{gas}} \sim 7.4 \times 10^3 \mathrm{M}_\odot$, while the gravitational softening at $z = 0$ is set to $\epsilon = 134$ pc[2]. The results presented in this paper

---

[2] These are representative values; in detail, they vary slightly from volume to volume.

| Simulation | Volume | $\mathbf{N}_{\mathrm{dwarf}}$ [all; $z=0$] | $\mathbf{N}_{\mathrm{dwarf}}$ [luminous; $z=0$] |
|---|---|---|---|
| APOSTLE: HYDRO & DMO | (1) | (2) | (3) |
| | Ap-V1 | 146 | 62 |
| | Ap-V4 | 240 | 83 |
| | Ap-V6 | 240 | 89 |
| AURIGA: MHD & DMO | | | |
| | Au-6 | 17 | 14 |
| | Au-16 | 35 | 31 |
| | Au-21 | 30 | 29 |
| | Au-23 | 19 | 19 |
| | Au-24 | 51 | 46 |
| | Au-27 | 26 | 24 |

**Table 1.** Number of isolated dwarf galaxies (see definition in Section 2.3) identified in the APOSTLE and AURIGA simulations. Column (2) lists *all* dwarf galaxy haloes in the appropriate mass range; column (3) lists the number of them that are *luminous*, i.e. those that have formed at least one star particle. The larger simulation volume in APOSTLE compared to AURIGA results in the presence of many more candidate dwarf haloes.

use the APOSTLE L1 simulations only; however, we have checked explicitly that the results are converged at L2 and L3.

The APOSTLE project was performed using the EAGLE simulation code (Schaye et al. 2015; Crain et al. 2015), a modified version of the massively parallel smoothed particle hydrodynamics (SPH) code, P-GADGET-3 (Springel 2005; Springel et al. 2008). The EAGLE code contains several updated subgrid physics models for the cooling and heating of gas (Wiersma et al. 2009a); star formation and reionisation (Schaye 2004; Schaye & Dalla Vecchia 2008); stellar mass loss and enrichment (Wiersma et al. 2009b), as well as the feedback from stars and AGN (Booth & Schaye 2009; Dalla Vecchia & Schaye 2012). A comprehensive discussion of the subgrid prescriptions and the effect of varying their parameters can be found in Schaye et al. (2015) and Crain et al. (2015). SPH quantities and hydrodynamic forces are computed using the ANARCHY SPH scheme (see Schaller et al. 2015b for details), itself based on the pressure-entropy SPH formulation described in Hopkins (2013). For the conversion of gas into stars, a density threshold $n_{\mathrm{sf}} = 0.1\,(Z/0.002)^{-0.64}$ cm$^{-3}$ is adopted in APOSTLE, where $Z$ is the gas metallicity. Furthermore, because the simulation is unable to adequately resolve or model the cold phase of the interstellar medium (ISM), a temperature floor of $\sim 10^4$ K is adopted, imposing an effective equation of state on the unresolved ISM. Finally, we note that the parameters for the subgrid implementation in the APOSTLE project correspond to the EAGLE REFERENCE model.

### 2.2 The AURIGA simulations

The AURIGA project (Grand et al. 2017) focuses specifically on re-simulations of Milky Way mass haloes, rather than the Local Group environment. Re-simulation candidates were chosen from the same 100 Mpc periodic box as the EAGLE project. To ensure a relatively isolated sample of Milky Way-like systems,

candidate haloes were required to have a present-day mass [3] $10^{12} < M_{200}/M_\odot < 2 \times 10^{12}$. The centre of a target halo is also required to be located outside $9 \times r_{200}$ of any other halo that has a mass greater than 3 per cent of the target halo mass. The parent volume and subsequent re-simulations assume cosmological parameters derived by *Planck* (Planck Collaboration et al. 2014): $\Omega_m = 0.307$, $\Omega_b = 0.04825$, $\Omega_\Lambda = 0.693$, $h = 0.6777$, $n_s = 0.9611$ and $\sigma_8 = 0.8288$. The cosmological parameters and input power spectrum are exactly the same as those used in the EAGLE project.

In total, 30 candidate haloes were selected for re-simulation: while all 30 have LR and MR versions, six of them have been re-simulated at high-resolution (HR, corresponding to 'Level 3' in the nomenclature of Grand et al. 2017). In this paper, these six haloes will be labelled as 'Au-6', 'Au-16', 'Au-21', 'Au-23', 'Au-24' and 'Au-27'. The HR AURIGA simulations are specified by $m_{DM} = 4 \times 10^4 M_\odot$, $m_{gas} \sim 6 \times 10^3 M_\odot$ and $\epsilon = 184$ pc. Nominally, the numerical resolution of both APOSTLE and AURIGA is comparable to or better than that of other works in the literature, which do report cores.

A significant difference between APOSTLE and AURIGA is that while the former uses the SPH approach to solve the hydrodynamics, AURIGA makes use of the magnetohydrodynamics (MHD) code, AREPO (Springel 2010), which implements a moving, unstructured Voronoi mesh to solve the MHD equations (Pakmor et al. 2014). In this sense, $m_{gas}$ in AURIGA refers to mass associated with a particular gas cell in the Voronoi mesh, rather than to the mass of an SPH particle. The moving mesh in AURIGA is adaptive, resolving regions of high density with many more cells of a smaller size than in low density environments.

In addition to the different approach to solving the hydrodynamics, the subgrid implementation in AURIGA is also somewhat different, deriving primarily from the treatment of gas cooling and heating, star formation, metal enrichment, stellar and AGN feedback laid out in Vogelsberger et al. (2013), Marinacci et al. (2014) and Pillepich et al. (2018a)[4]. The density threshold for star formation $n_{sf} = 0.13$ cm$^{-3}$ in AURIGA, although, unlike in APOSTLE, there is no explicit dependence of this threshold on the metallicity of the star forming gas. As in APOSTLE, a temperature floor of $\sim 10^4$ K is also adopted. The AURIGA model also includes a simple prescription for the self-shielding of dense gas ($> 10^{-3}$ cm$^{-3}$) from background ultraviolet radiation; self-shielding is not modelled in APOSTLE.

There are also differences in the manner in which supernova feedback is implemented in the respective models. APOSTLE follows the scheme outlined in Dalla Vecchia & Schaye (2012), in which energy from supernovae is dumped stochastically in a thermal component only, resulting in a constant temperature increase of gas particles receiving this energy by an amount $\Delta T = 10^{7.5}$ K. The resulting energy injected per stellar mass formed depends on local properties of the gas (i.e. its density and metallicity). On the other hand, AURIGA uses the method of Marinacci et al. (2014) to deposit feedback energy as kinetic and thermal components in equal parts. This feedback is modelled by converting gas cells in

wind particles, where the wind velocity is set to $3.64\sigma_{DM}^{1D}$; here $\sigma_{DM}^{1D}$ is the local 1D DM velocity dispersion (c.f. Okamoto et al. 2010).

Finally, we note that every volume re-simulated as part of the APOSTLE and AURIGA projects have DMO counterparts simulated from the same set of initial conditions. This is particularly important as our goal is to study the effect of galaxy formation physics on the inner structure of dark matter haloes compared to collisionless simulations.

## 2.3 Definitions and sample selection

A post-processing step common to both APOSTLE and AURIGA is the identification of haloes and subhaloes. First, haloes are identified using the 'friends-of-friends' (FOF) algorithm, in which dark matter particles separated by at most 0.2 times the mean inter-particle separation are linked together to form groups (Davis et al. 1985). Within each group, sets of gravitationally bound substructures are identified using the SUBFIND algorithm (Springel et al. 2001). This splits a FOF halo into a 'main' halo and its associated subhaloes: one can think of this as the distinction between the hosts of 'central' and a 'satellite' galaxies. In what follows, we will be concerned with the 'main' halo of FOF groups only. We determine the centres of haloes using the *shrinking sphere* method (e.g. Power et al. 2003), which identifies the density maximum of a self-bound structure by recursively computing the centre of mass of all DM particles within a shrinking sphere, until a convergence criterion is met. In each iteration, the radius of the sphere is reduced by 5 per cent, and stopped when only 1000 particles or 1 per cent of the particles of the initial sphere (whichever is smaller) are left. In the vast majority of cases, the shrinking sphere centre coincides with the location of the particle with the minimum value of the gravitational potential identified by SUBFIND.

In what follows, we will be concerned primarily with the haloes of *isolated* dwarf galaxies. Isolated (or 'field') haloes are objects found at a distance greater than 300 kpc away from the main galaxy (i.e. the Milky Way analogue). In the case of APOSTLE, we require an isolated halo to be more than 300 kpc away from both the Milky Way *and* M31 analogues. As these criteria are enforced at $z = 0$, our selection will inevitably include a small fraction ($\sim 20\%$) of "backsplash" galaxies: those that were once part of a larger host, but are not any longer. A dwarf galaxy is defined as being in the mass range $10^9 < M_{DM}/M_\odot < 5 \times 10^{10}$, where $M_{DM}$ is the bound DM mass associated with the isolated galaxy as identified by SUBFIND. The properties of non-isolated, satellite galaxies have been presented in detail by Fattahi et al. (2016a, 2018) for APOSTLE and by Simpson et al. (2018) for the AURIGA simulations.

Table 1 lists the total number of objects satisfying these criteria in the various simulation volumes. Given this choice of mass range and the resolution of APOSTLE HR and AURIGA HR, the minimum number of particles used to compute DM density profiles is $\sim 25\,000$, which is more than sufficient to resolve accurately the dynamics of the inner part of the DM halo, which is the scale of interest. When we refer to stellar mass, $M_\star$, of a galaxy, we include all star particles identified by SUBFIND as being gravitationally bound. Finally, we exclude any objects that may be contaminated by the presence of heavier, low-resolution DM particles – this is often the case for haloes located too close to the boundary of the high-resolution region of the simulation volume. This is achieved by restricting our selection to only dwarfs that are located within a sphere of radius 1 Mpc from the centre of the main galaxy in

---

[3] Here, the mass, $M_{200}$, is defined as the mass contained within the radius, $r_{200}$, which encompasses a mean matter density equal to 200 times the critical density of the Universe at a given redshift.

[4] Note that while stellar winds are treated as in the ILLUSTRISTNG model (Pillepich et al. 2018a), AURIGA uses the AGN prescription from the original ILLUSTRIS model. We do not expect AGNs to play a significant role in the present analysis.
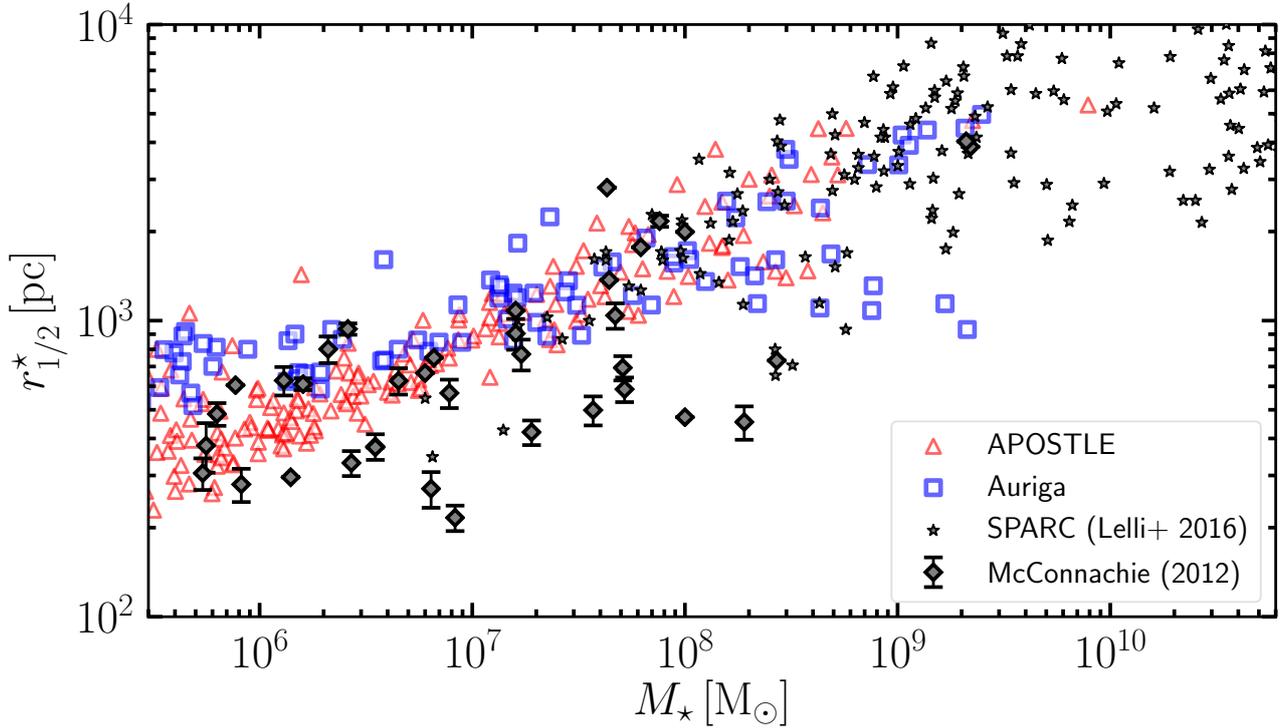
**Figure 1.** Galaxy stellar half-mass radius, $r_{1/2}^\star$, versus stellar mass, $M_\star$, for isolated galaxies identified in the three high-resolution APOSTLE volumes, and the six high-resolution AURIGA volumes. The stellar mass of each galaxy is defined as the total mass in stars bound to the halo as determined by SUBFIND. The grey diamonds with error bars show the published data compiled for the isolated Local Group dwarfs by McConnachie (2012), while the stars represent galaxies from the SPARC sample compiled by Lelli et al. (2016).

AURIGA (3 Mpc from the Local Group barycentre in the case of APOSTLE). We have also checked explicitly that no low-resolution particles are associated with haloes included in the final selection.

To match the isolated haloes between the DMO and hydrodynamical runs, we use a bijective matching procedure: first, we consider the 50 most-bound DM particles from a candidate halo in the hydrodynamical run, and look for the DMO halo in which there are at least 25 (50 per cent) of these particles. The match is then confirmed by repeating the same process, this time starting with the DMO haloes.

An important characteristic of this work is that while both APOSTLE and AURIGA are re-simulations of 'special' environments, (1) they are fully cosmological in nature (i.e. the large-scale tidal fields appropriate to the 100 Mpc volumes they were extracted from are self-consistently followed albeit at lower resolution), and (2) the subgrid prescriptions have been shown to produce realistic galaxy populations (i.e. in agreement with a wide range of observational data, across a range of redshifts) in larger simulation volumes. Point (2) in particular is not trivial: for example, a zoom simulation in which the subgrid parameters are tuned to reproduce properties of dwarf galaxies on Local Group scales is not guaranteed to reproduce the galaxy stellar mass function, colour distribution, galaxy size-mass relation etc. observed among galaxies in the field. The subgrid models used in APOSTLE and AURIGA are very similar to those used by the EAGLE (Schaye et al. 2015) and ILLUSTRIS (Vogelsberger et al. 2014) simulations, respectively; the galaxy formation models have not been tuned specifically to reproduce properties of the Milky Way or galaxies in the Local Group.

To demonstrate that the reverse is also true (i.e. that the chosen subgrid parameters are appropriate for the resolution / regime of interest in this paper), in Fig. 1 we present the galaxy size-stellar mass relation for isolated dwarfs in APOSTLE (see also Campbell et al. 2017) and AURIGA. Galaxy size in this plot is the (3D) stellar half-mass radius, $r_{1/2}^\star$, while the stellar mass is the total mass in star particles bound to the halo. We only display the relations for isolated dwarf galaxies using the criteria set out at the start of this subsection. For comparison, the grey diamonds with error bars show the data for isolated dwarf galaxies in and around the Local Group compiled by McConnachie (2012). We additionally include data from the SPARC galaxy sample (Lelli et al. 2016) shown in the grey stars. McConnachie (2012) measures the half-light radius along the semi-major axis of each galaxy, while the values measured in the simulations are spherical calculations based on the 3D distribution of stars. To aid the comparison between simulated dwarfs and the data, we have converted the observed projected half-light radius into the equivalent 3D half-light radius by multiplying by a factor of 4/3. While the simulations reproduce the general trend seen in the data, they do not reproduce the scatter at fixed stellar mass. However, the level of agreement between our simulations and the data is comparable to that observed in other hydrodynamical simulations of dwarf galaxies (see, e.g. Fig. 1 in Fitts et al. 2017). Both AURIGA and APOSTLE simulations show a paucity of small, compact galaxies ($r_{1/2}^\star < 400$ pc) in the range $10^6 \mathrm{M}_\odot < M_\star < 10^8 \mathrm{M}_\odot$. However, these sizes are smaller than the minimum resolution with which we are able to measure density profiles in this work (the 'convergence radius' of the halo; see Sec-
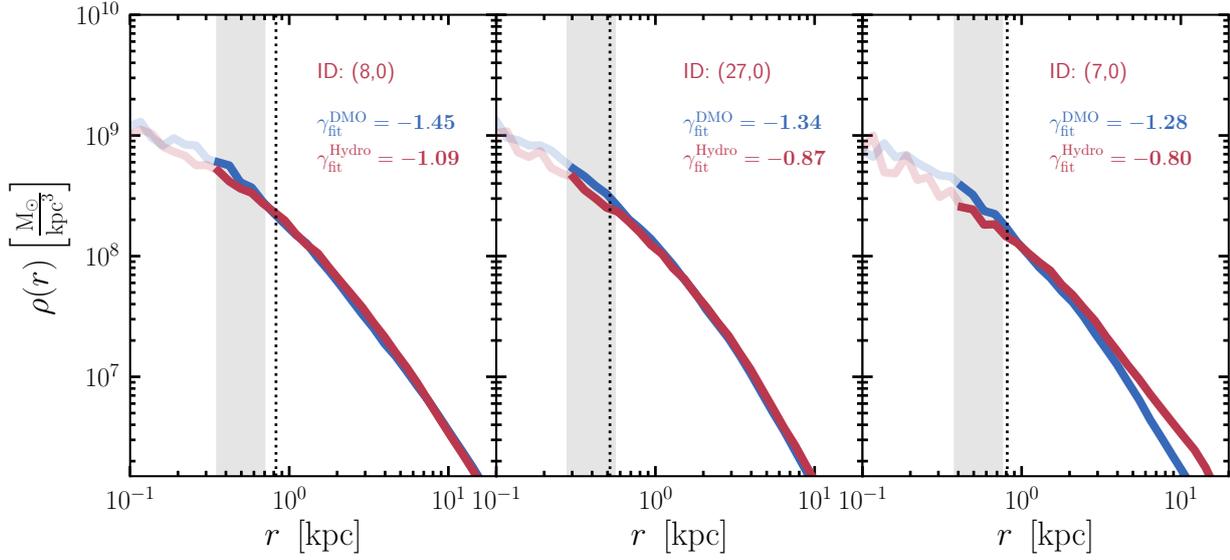
**Figure 2.** Dark matter density profiles of the isolated dwarf galaxy halo that exhibits the shallowest inner slope, $\gamma_{\rm fit}$, in each of the three hydrodynamical APOSTLE HR runs at $z = 0$ (V1, V4 and V6 from left to right). In each panel, the thick red line shows the density profile of the dark matter component in the run with full hydrodynamics and the thick blue line the density profile of this halo's counterpart in the DMO version of this simulation. Linestyles are drawn faint below the convergence radius of the halo. The vertical dotted line marks 1 per cent of the halo virial radius. The values of $\gamma_{\rm fit}$ (as defined in the main text) in the DMO and hydrodynamical versions of this halo are compared in the top right corner of each panel; the portion of the profile that is fit to derive $\gamma_{\rm fit}$ is highlighted by the shaded grey band. Properties of these dwarfs are listed in Table 2.
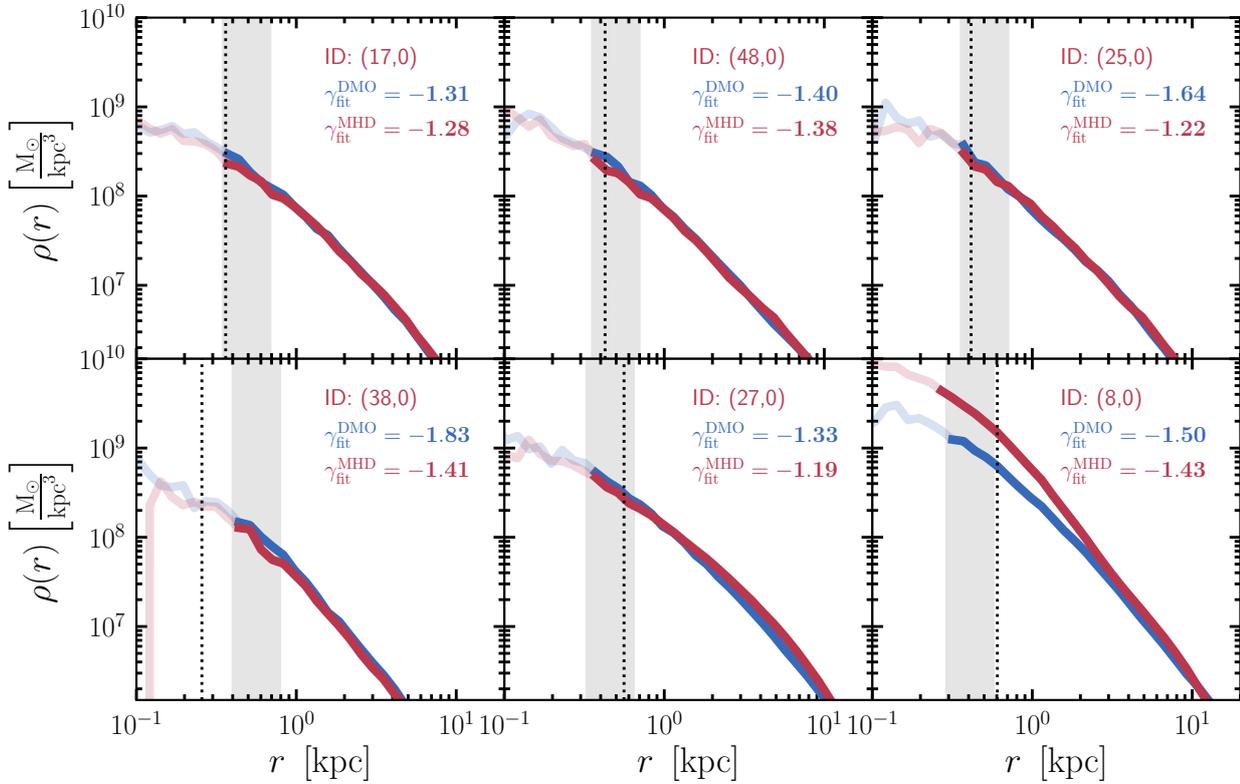


**Figure 3.** Same as Fig. 2, but for the six AURIGA HR haloes (Au-6, 16, 21, 23, 24 and 27 from left to right starting from the upper left panel).

| Simulation | (Volume, FOF, Subhalo ID) | $M_{\rm DM}^{\rm DMO}$ $[{\rm M_\odot}]$ | $M_{\rm DM}^{\rm Hydro}$ $[{\rm M_\odot}]$ | $M_\star/M_{\rm DM}^{\rm Hydro}$ |
|---|---|---|---|---|
| APOSTLE: | (1) | (2) | (3) | |
| | (Ap-V1, 8,0) | $6.5 \times 10^{10}$ | $5.3 \times 10^{10}$ | 0.014 |
| | (Ap-V1, 38, 0) | $1 \times 10^{10}$ | $8 \times 10^9$ | 0.0084 |
| | (Ap-V4, 22,0) | $1.8 \times 10^{10}$ | $1.5 \times 10^{10}$ | 0.0039 |
| | (Ap-V4, 27,0) | $1.6 \times 10^{10}$ | $1.4 \times 10^{10}$ | 0.0039 |
| | (Ap-V6, 7,0) | $6.2 \times 10^{10}$ | $7.2 \times 10^{10}$ | 0.0045 |
| AURIGA: | | | | |
| | (Au-6, 17,0) | $5.4 \times 10^9$ | $4.5 \times 10^9$ | 0.0044 |
| | (Au-16, 47,0) | $7.6 \times 10^9$ | $6.6 \times 10^9$ | 0.0042 |
| | (Au-16, 48,0) | $8.9 \times 10^9$ | $7.3 \times 10^9$ | 0.0021 |
| | (Au-21, 25,0) | $8.2 \times 10^9$ | $6.7 \times 10^9$ | 0.002 |
| | (Au-21, 32,0) | $4.7 \times 10^9$ | $3.6 \times 10^9$ | 0.0018 |
| | (Au-23, 15,0) | $8.1 \times 10^9$ | $6.8 \times 10^9$ | 0.007 |
| | (Au-23, 38,0) | $1.9 \times 10^9$ | $1.4 \times 10^9$ | $7.8 \times 10^{-6}$ |
| | (Au-24, 27,0) | $2.0 \times 10^{10}$ | $1.8 \times 10^{10}$ | 0.017 |
| | (Au-24, 52,0) | $9.8 \times 10^9$ | $8.3 \times 10^9$ | 0.011 |
| | (Au-27, 8,0) | $2.6 \times 10^{10}$ | $2.2 \times 10^{10}$ | 0.098 |
| | (Au-27, 19,0) | $8.8 \times 10^9$ | $7.4 \times 10^9$ | 0.0042 |

**Table 2.** A list of properties for isolated dwarfs that are given individual attention in this paper. A dwarf is identified uniquely using the numbers in parentheses provided in column (1), which follows the format: (Volume #, FOF #, subhalo #). Column 2 lists the mass in DM contained in the DMO counterpart of this halo, while column 3 lists the equivalent value in the run with hydrodynamics. Finally, column 3 lists the stellar-to-halo mass ratio for each dwarf.

tion 3.1); as such, the absence of these galaxies is not expected to impact the remainder of our analysis in any significant way.

## 3 RESULTS

In this section, we present the main results of this work. In particular, we compare the DM density profiles (Section 3.1) and star formation histories (Section 3.4) of isolated dwarf galaxies (using the criteria outlined in Section 2.3) identified in the APOSTLE and AURIGA simulations.

### 3.1 The ubiquitous cuspy density profile

We begin by analysing the shape of DM density profiles of isolated dwarfs in the APOSTLE and AURIGA simulations. Fig. 2 shows the density profiles of the dwarf galaxy haloes exhibiting the *shallowest* inner slope in APOSTLE-HYDRO at $z = 0$. The inner slope is quantified by a parameter, $\gamma_{\rm fit}$, which is the power law index that best fits the density profile in the range $r_{\rm conv} < r < 2.0 \, r_{\rm conv}$, where $r$ is the radial distance from the halo centre, while $r_{\rm conv}$ is the convergence radius defined according to Power et al. (2003), and is the radius within which the relaxation time is $\sim 1/3$ the age of the Universe. This is similar to the procedure followed by e.g. Chan et al. (2015); El-Badry et al. (2017); Macciò et al. (2017), although these authors typically fit the range between 1-2 per cent of the halo virial radius. Our choice of $r_{\rm conv}$ is motivated by the fact that this is the innermost radius of the DM density profile that is numerically well converged given the number of particles in the halo – the profiles shown in Fig. 2 are drawn with faint lines below this limit. This figure also shows that the scale corresponding to 1

per cent the halo's virial radius (vertical dotted lines) is sometimes located below $r_{\rm conv}$, and at other times does not probe the innermost (resolved) part of the profile, further motivating our choice to define $\gamma_{\rm fit}$ in a range defined by $r_{\rm conv}$. In each panel, the thick red line represents the DM density profile in APOSTLE-HYDRO, while the thick blue curve is the density profile measured for this halo's counterpart in APOSTLE-DMO.

Fig. 2 shows that, according to the values of $r_{\rm conv}$, the DM density profiles of APOSTLE are reliable for $r \gtrsim 400$ pc. As expected, our selection of the shallowest APOSTLE-HYDRO density profiles yields systems with slightly lower central densities than in APOSTLE-DMO (within $\lesssim 1$ kpc). However, even the profiles with the shallowest slopes in APOSTLE-HYDRO show no evidence of cores, at least larger than 400 pc in size. In fact, the shallowest slope we measure is $\gamma_{\rm fit} = -0.80$, associated with a $7.2 \times 10^{10} {\rm M_\odot}$ halo in Ap-V4 (right panel of Fig. 2).

The shallowest profiles from AURIGA-MHD are shown in Fig. 3. Convergence in the density profiles is reached at a comparable radial scale as in APOSTLE. While the central densities are reduced in the runs with MHD relative to DMO (with the exception of the dwarf galaxy selected from Au-27, shown in the bottom right panel of Fig. 3), once again, no cores are present. Table 2 lists the properties of these dwarfs in both simulations. It is interesting to note that the dwarf galaxy haloes with the shallowest DM density profiles display a wide range of star formation efficiencies, as measured by their stellar-to-halo mass ratio, $M_\star/M_{\rm DM}$, which ranges from $8 \times 10^{-6}$ in Au-23 to $\sim 1.5 \times 10^{-2}$ in Ap-V1 and Au-24.
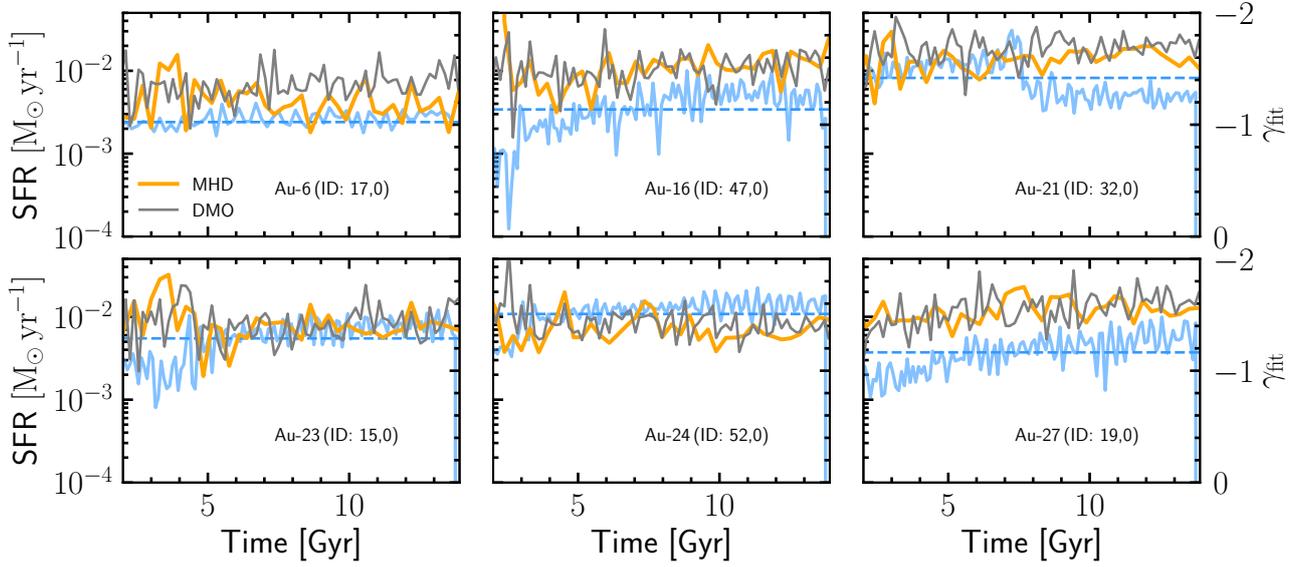
**Figure 4.** Time evolution of the best-fit inner slope, $\gamma_{\rm fit}$, of the dark matter density profile in the hydrodynamical version of an isolated dwarf galaxy halo (orange), and its DMO counterpart (grey) identified in each of the six AURIGA volumes. The blue curve shows the time variation of the star formation rate (smoothed over 100 Myr) of the galaxy formed in this halo. The horizontal blue dashed line marks the mean star formation rate averaged over the entire history of this galaxy. In each panel, we have chosen to display these relations for the isolated dwarf galaxy with the greatest stellar mass at $z = 0$ i.e. the halo with the highest *average* star formation rate in each simulation. Properties of these dwarfs are listed in Table 2.
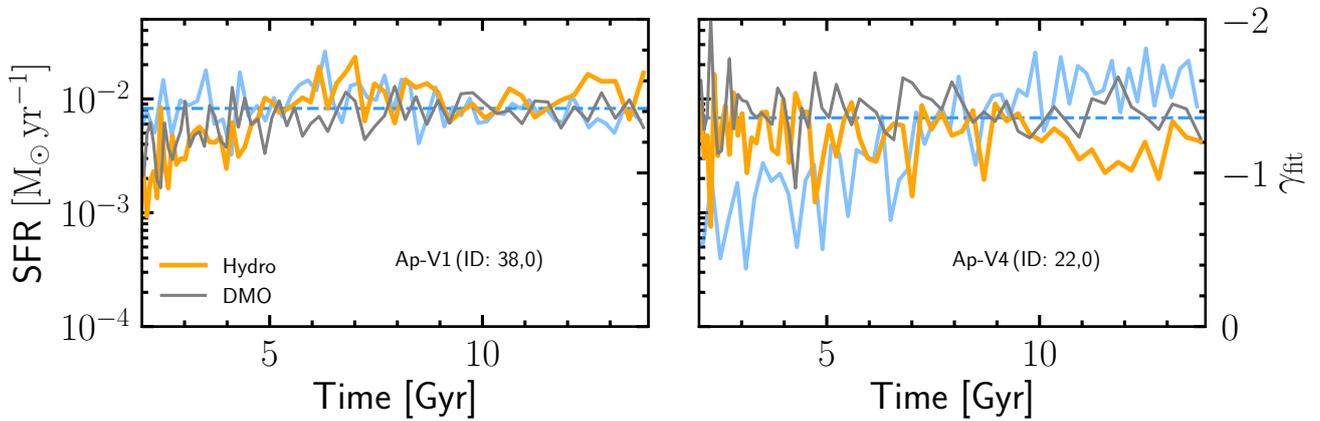


**Figure 5.** As Fig. 4 for APOSTLE volumes Ap-V1 and Ap-V4.

## 3.2 Cusps and bursty star formation

As discussed in Section 1, core formation in the literature has been ascribed to energetic processes associated with galaxy formation, such as repeated outbursts of supernovae, and the existence of bursty and sustained periods of high star formation rates (SFRs). A particularly interesting connection between SFRs and the shape of the DM density profile was demonstrated by El-Badry et al. (2017), who found a strong anti-correlation between the two in high-resolution simulations of dwarf galaxies; where periods of bursts in the SFR were associated with a flattening of $\gamma_{\rm fit}$, whereas a steeper value of $\gamma_{\rm fit}$ was restored during more quiescent phases.

Simulations performed by Read et al. (2016) also find differences in the rotation curve of dwarf galaxies induced by episodes of starbusts and quiescence.

To examine if such a correlation can be identified in our simulations, in Fig. 4 we plot the time evolution of $\gamma_{\rm fit}$ for a selection of isolated dwarfs from AURIGA-DMO (grey curves) and AURIGA-MHD (orange curves), and their associated SFRs (blue curves). We have specially selected isolated dwarfs from AURIGA-MHD that have the highest stellar mass at $z = 0$. While the merger tree of a galaxy can be traversed to trace the growth of stellar mass and measure the SFR, the resolution of this method is limited by the spacing of simulation snapshots. On the other hand, the age of a
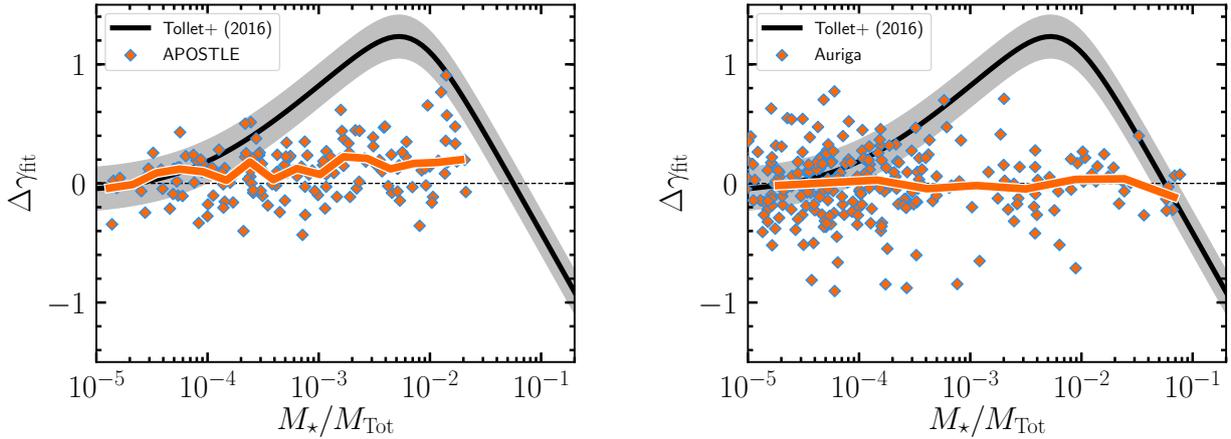
**Figure 6.** Change in the best-fit inner slope of the dark matter density profile, $\gamma_{\rm fit}$, between isolated APOSTLE (left panel) and AURIGA (right panel) haloes and their matched DMO counterparts, as a function of stellar-to-total halo mass ratio. Negative values correspond to steeper dark matter density profiles in the hydrodynamical runs, while positive values correspond to profiles that have become shallower in the hydrodynamical runs. Each diamond represents an individual halo, while the solid line shows the median relation. The solid black curve is obtained using the fitting function proposed by Tollet et al. (2016), building on a similar relation previously suggested by Di Cintio et al. (2014); here we have assumed $\gamma_{\rm fit}^{\rm DMO} = -1.5$.

The grey band represents a $1\sigma$ scatter of 0.18 around the mean relation.

stellar population is output at the exact timestep corresponding to its birth. This means that for all stars identified in a galaxy at a particular time, the snapshots contain information on the exact scale factor at which this star was born; this information can be used to create a star formation history (SFH) with as good a time resolution as it is possible to obtain from the simulations. In what follows, we always measure SFRs/SFHs using the latter definition. In Fig. 4, the SFR of each galaxy has been smoothed over a 100 Myr interval.

The specific SFRs for our selection of AURIGA-MHD dwarfs are comparable (and, in some cases, larger) than those reported by Fitts et al. (2017) and El-Badry et al. (2017). From Fig. 4, we find that in no case does the value of $\gamma_{\rm fit}$ ever become shallower than $\approx -1$; in fact, the evolution of $\gamma_{\rm fit}$ is largely identical in AURIGA-MHD and AURIGA-DMO. In other words, the effect of the hydrodynamics, if any, on the shape of the DM density profile is *comparable to the natural variation of the inner slope* (due to mergers and accretion) that one measures from a purely collisionless simulation. Fig. 4 therefore shows that in the six AURIGA-MHD simulations, even transient cores (i.e. those that form temporarily, before reverting to a cusp) never form. As shown in Fig. 5, we find similar results for haloes in the APOSTLE simulation.

### 3.3 Cusps and galaxy formation efficiency

Several authors have reported a positive correlation between the value of the inner slope of the DM density profile (i.e. $\gamma_{\rm fit}$) and the star forming efficiency of a halo, measured by its stellar-to-halo mass ratio (e.g. Governato et al. 2012; Di Cintio et al. 2014; Macciò et al. 2017). In principle, such a suggestion is reasonable: if star formation and/or feedback is responsible for altering the shape of the DM density profile, haloes with larger stellar-to-halo mass ratio are more likely to be affected as there is effectively more energy available from supernovae to unbind the dark matter. Furthermore, Fitts et al. (2017) find that, in their simulations, the half-mass radius of the galaxy sets a characteristic length scale which determines the size of the core formed in the DM density profile.

Fig. 6 investigates the relationship between $\gamma_{\rm fit}$ and $M_\star/M_{\rm Tot}$ (where $M_{\rm Tot}$ is the total halo mass including DM, gas and stars) in

APOSTLE and AURIGA. Rather than simply plotting $\gamma_{\rm fit}$ from the hydrodynamical run on the vertical axis (as is commonly done in the literature), we plot $\Delta\gamma_{\rm fit} = \gamma_{\rm fit}^{\rm Hydro} - \gamma_{\rm fit}^{\rm DMO}$ i.e. the *change* in the inner slope between a matched pair of hydro / DMO haloes. The reason for this is that smaller haloes, which are less well resolved, will naturally yield more 'negative' values of $\gamma_{\rm fit}$ as $r_{\rm conv}$ in these haloes will be closer to the scale radius of the profile, where the slope $\approx -2$. For larger haloes, which are resolved with many more particles, $r_{\rm conv}$ is pushed 'further in' towards the halo centre where the typical slope is closer to $\approx -1$. As low-mass haloes, on average, have low star forming efficiency, one would measure a positive correlation between $\gamma_{\rm fit}$ and $M_\star/M_{\rm Tot}$ that is in reality is just an artefact. As defined, *negative* values of $\Delta\gamma_{\rm fit}$ correspond to profiles that have become *steeper* in the simulation with hydrodynamics, while *positive* values of $\Delta\gamma_{\rm fit}$ correspond to haloes where the slope is *shallower* after the inclusion of baryons.

The orange lines in Fig. 6 show the median trend. Given the relatively small number of isolated dwarfs in the two simulations and the scatter in $\Delta\gamma_{\rm fit}$, the median trend is noisy. However, there is no obvious trend of $\Delta\gamma_{\rm fit}$ with $M_\star/M_{\rm Tot}$; the variations are consistent with zero. For comparison, we have also included the relationship inferred from simulations by Di Cintio et al. (2014) and Tollet et al. (2016), which shows a clear variation in $\Delta\gamma_{\rm fit}$ as a function of $M_\star/M_{\rm Tot}$. In making this comparison with Tollet et al. (2016), we have assumed $\gamma_{\rm fit}^{\rm DMO} = -1.5$.

The density profiles shown in Figs. 2 and 3 show no significant deviation from an NFW shape, and lack a characteristic length scale that may be imposed by the galaxy half-mass radius ($r_{1/2}^\star$) on the host halo DM profile. We remind the reader that the size-mass relations of isolated dwarfs in both APOSTLE and AURIGA are consistent with the data (Fig. 1). Furthermore, for galaxies with $M_\star > 10^7 {\rm M}_\odot$, $r_{1/2}^\star \gtrsim 600$ pc $\approx 1.5\, r_{\rm conv}$ in both APOSTLE and AURIGA, so any potential scale imprinted on the DM density profile would have been adequately resolved in our simulations.
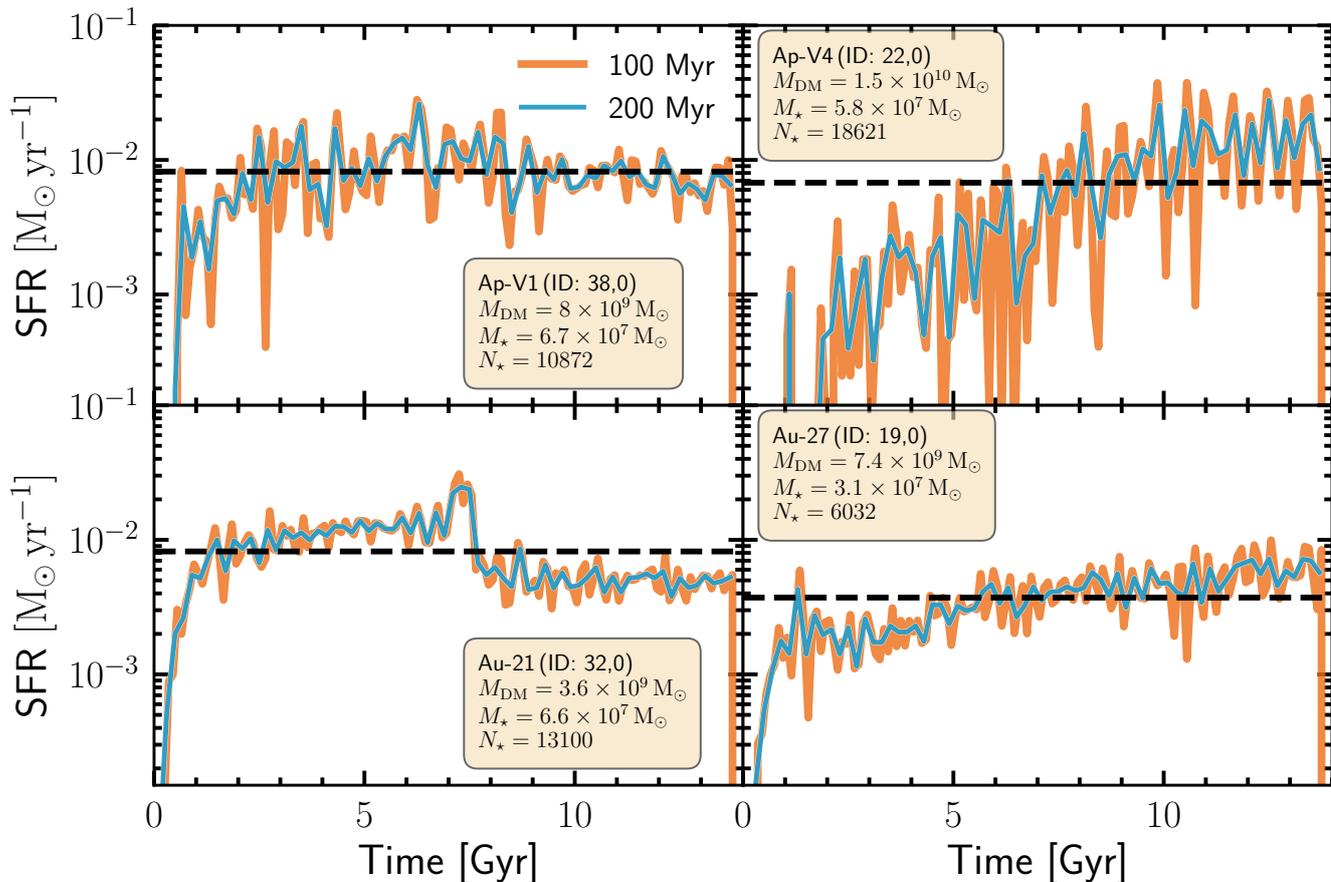
**Figure 7.** Individual star formation histories (SFHs) for a selection of isolated dwarf galaxy haloes from APOSTLE (top row) and AURIGA (bottom row). These galaxies were selected to have the highest average SFR amongst all isolated dwarfs at $z = 0$ in the volume from which they are chosen. After collecting the set of stars present in each galaxy at $z = 0$, the expansion factor at which the star particle was born is used to construct the SFH. The orange and blue lines respectively show the SFHs smoothed over 100 and 200 Myr time intervals. The dashed horizontal line marks the average star formation rate of the galaxy in each panel.

### 3.4 Cusps and star formation history diversity

Next, we proceed to examine the star formation histories (SFHs) of the isolated dwarfs identified in our simulations. In Fig. 7, we show the evolution of SFRs for a selection of individual galaxies from APOSTLE-HYDRO (top panel) and AURIGA-MHD (bottom panel). The orange and blue lines, respectively, show the SFRs averaged over 100 and 200 Myr time bins. We have chosen isolated dwarf galaxies that have the largest $z = 0$ stellar mass in the volume from which they are extracted. It is interesting to observe the appreciable fluctuations in the SFRs of these galaxies, particularly in the case of the APOSTLE-HYDRO dwarfs. For example, the galaxy selected from Ap-V4 shows fluctuations in SFR of over two orders of magnitude over 100 Myr intervals. The dwarf galaxies from AURIGA-MHD also show big temporal variations in SFR, although these galaxies are not as bursty as those in APOSTLE-HYDRO. We have checked explicitly that the burstiness is not due to stochastic sampling in the star formation prescription: typically, each time bin in the smoothed SFH contains hundreds of newly-formed star particles, while the time intervals over which star formation is averaged are well above the length of a typical timestep taken in the simulation.

For objects of similar mass, Sparre et al. (2017) found that

galaxies in the FIRE simulations display strong, short bursts of star formation over 10 Myr timescales. When comparing the SFRs of APOSTLE and AURIGA galaxies smoothed over 10-50 Myr timescales we find that, in general, the dwarfs in our simulations exhibit more gentle SFR fluctuations than in FIRE, where galaxies show a stronger post-burst phase (i.e. a burst of star formation in the last ∼ 200 Myr or so of evolution). Recently, Dutton et al. (2018) have also reported larger SFR fluctuations in core-forming dwarfs than that measured in the cuspy dwarfs from APOSTLE and AURIGA. This is, in part, due to the different timescales over which the SFR is averaged: Dutton et al. (2018) average SFR over ∼5 Myr, which is considerably shorter than our choice of 100-200 Myr. Our conservatism is motivated by the desire to stay clear of the regime in which the stochastic formation of indvidual star particles may manifest as burstiness. In any case, we do not believe that this difference in the degree of SFR burstiness is the reason for the lack of cores in the simulations we have presented: indeed, as Benitez-Llambay et al. (2018) have shown, even extremely bursty dwarfs may continue to exhibit cuspy DM density profiles (see also Revaz & Jablonka 2018, and the discussion in Section 4).

It is natural to ask if the fluctuations in the SFR of the APOSTLE and AURIGA galaxies seen in Fig. 7 are compatible with the inferred SFHs of dwarfs observed in the Local Group. Fig. 8 shows
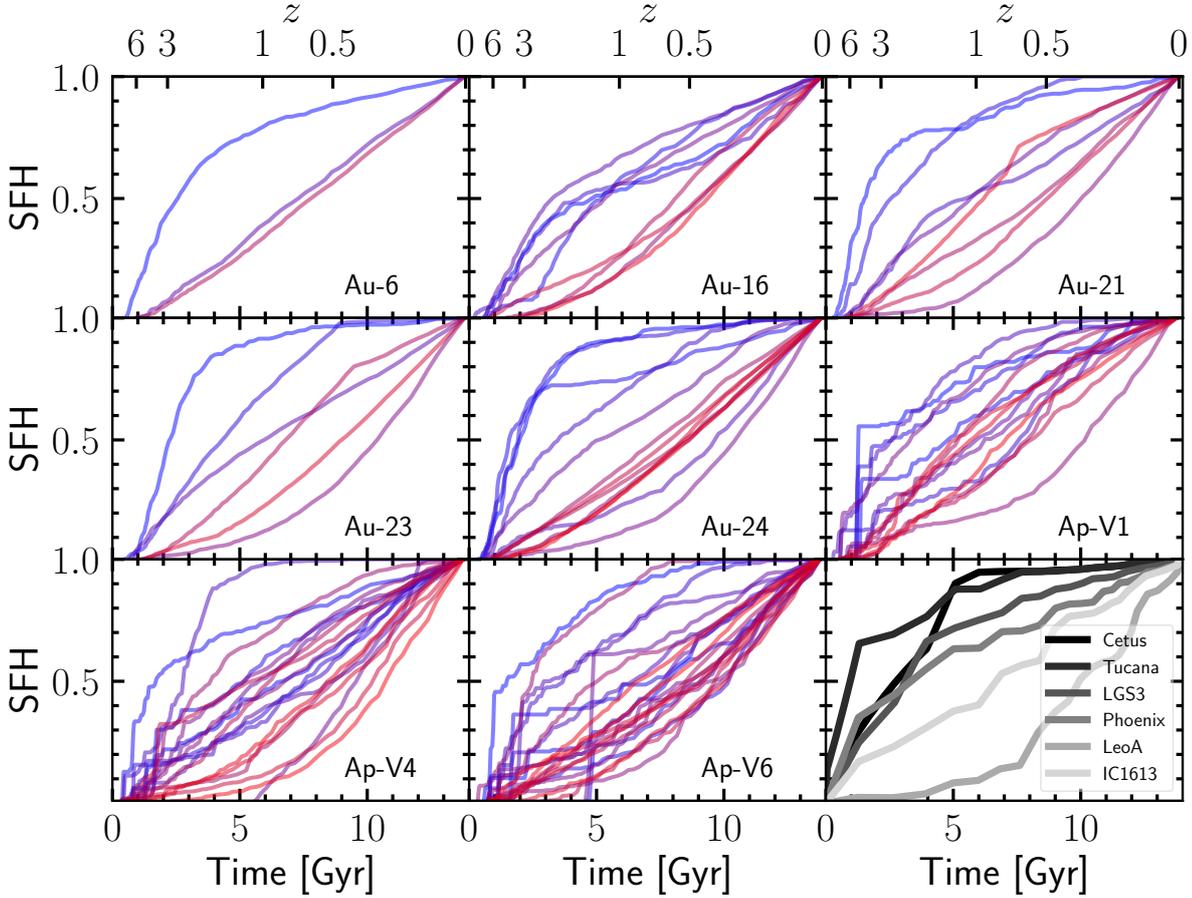
**Figure 8.** Cumulative SFHs for all isolated dwarf galaxies in the mass range $10^9 < M_{\mathrm{DM}}/\mathrm{M}_\odot < 5 \times 10^{10}$ and $10^6 < M_\star/\mathrm{M}_\odot < 10^8$ in the AURIGA (panels 1-5) and APOSTLE HR runs (panels 6-8). As in Fig. 7, the SFHs are constructed using the stellar birth time of star particles identified at $z = 0$ in each galaxy. The colour of each line, from blue to red, ranks galaxies in ascending order of present day stellar mass. To compare with the SFHs from our simulations, the last panel also displays the SFHs measured for real dwarf galaxies by Skillman et al. (2014).

the cumulative SFHs of dwarf galaxies in AURIGA-MHD (panels 1-5) and APOSTLE-HYDRO (panels 6-8) having stellar mass $10^6 < M_\star/\mathrm{M}_\odot < 10^8$ at $z = 0$; each curve represents a single galaxy. The final panel in this figure displays measured SFHs for real dwarf galaxies compiled by Skillman et al. (2014), who infer stellar ages by fitting the colour-magnitude diagrams assuming a stellar population synthesis model. The selection on stellar mass applied in Fig. 8 is consistent with the stellar masses of the galaxies in the Skillman et al. (2014) dataset.

Dwarf galaxies in both sets of simulations exhibit very diverse SFHs. The comparatively smaller simulation volume in AURIGA compared to APOSTLE results in fewer galaxies satisfying our criteria for isolated dwarfs in the appropriate stellar mass range. While the majority show sustained stellar mass growth throughout cosmic time, there are populations of dwarfs that are early forming (in which, for example, 80 per cent of the mass has been accumulated by $z = 3$) and late forming (more than half of the mass is accumulated after $z = 0.5$). The diverse SFHs are broadly comparable to those of observed Local Group dwarfs shown in the final panel of Fig. 8.

Another important observation can be made from Figs. 7 and 8. It is clear from Fig. 7 that galaxies in AURIGA-MHD typically have more quiescent SFHs than galaxies in APOSTLE-HYDRO. Yet, the *cumulative* SFHs in both simulations are similar. This demonstrates that the integrated SFH cannot inform us of whether the *differential* version of the SFH (as in Fig. 7) is bursty or not. Both bursty and comparatively quiescent SFHs can match the integrated SFHs inferred from the data; however, this agreement does not reveal which, if any, SFH is more realistic.

## 4 DISCUSSION

In Section 3.1 and 3.4, we have found that even though isolated dwarf galaxies in APOSTLE and AURIGA have bursty SFHs (comparable to those in other papers in the literature), their DM haloes do not form cores – at least not with a size $\gtrsim 400$ pc, which is the nominal resolution (determined by the convergence radius) at which our density profiles are reliable. Core formation in hydrodynamical simulations is attributed to late-time bursts of star for-

mation and the resulting gas motions that cause fluctuations in the gravitational potential of the DM (e.g. Pontzen & Governato 2012). In this section, we estimate the energy released by supernovae in our simulations and discuss why cores do not form in them.

The relevant timescale for inducing lasting changes to the DM density profile is the dynamical time of the halo at the spatial scale of interest, $t_{\rm dyn}$. We now make an estimate of the energy released by supernovae in APOSTLE and AURIGA dwarfs over a dynamical time at $\sim 1$ kpc, which corresponds roughly to the core size of interest.

Both sets of simulations adopt a Chabrier stellar initial mass function (IMF). Assuming that only stars with mass 8-100 $M_\odot$ explode in core-collapse supernovae, and that each supernova releases $\sim 10^{51}$ ergs of energy, we estimate that energy of the order of $\sim 2 \times 10^{49}$ ergs/$M_\odot$ is injected per stellar mass in stars formed. Within the dynamical time at 1 kpc from the halo centre, a galaxy is able to produce at most $\Delta M_\star = {\rm SFR} \times t_{\rm dyn}^{\rm 1kpc}$, where SFR is the star formation rate of the galaxy during this period. The total energy available from supernovae is then:

$$
\begin{aligned}
E_{\rm SN} &= 2 \times 10^{49} {\rm ergs} \cdot \Delta M_\star \\
&= 2 \times 10^{49} {\rm ergs} \cdot {\rm SFR} \times t_{\rm dyn}^{\rm 1kpc},
\end{aligned}
\tag{1}
$$

where $E_{\rm SN}$ is the energy released in supernovae following the formation of $\Delta M_\star$ in stellar mass. Inserting typical values for the SFR and $t_{\rm dyn}^{\rm 1kpc}$ for $\sim 10^{10} M_\odot$ dwarfs in AURIGA and APOSTLE, we obtain $E_{\rm SN} \sim \mathcal{O}(10^{55})$ ergs (the precise value for an individual galaxy will depend on its SFR and the concentration of its host halo)[5]. While only a fraction of this energy will couple to the DM, the total energy budget available from star formation in these simulations is consistent with estimates in the literature (e.g. Pontzen & Governato 2012; Peñarrubia et al. 2012; Chan et al. 2015), and of a similar order of magnitude to the gravitational work needed to unbind a cusp into a core. This, combined with our findings in Section 3, demonstrates that bursty SFHs and feedback from supernovae are *not*, by themselves, *sufficient* conditions for forming cores in dwarf galaxy haloes.

One reason that may explain, at least in part, why both AURIGA and APOSTLE fail to produce cores can be traced back to the observation made by Governato et al. (2010) that the core-forming ability of a simulated dwarf galaxy is also sensitive to the gas density threshold for star formation, $n_{\rm sf}$, assumed in the simulation. The interpretation is that with a higher star formation threshold, more gas is allowed to collect at the centre of a DM halo, eventually resulting in the gas density exceeding the local DM density. When star formation eventually occurs, the resulting gas outflow in a simulation with a high threshold is more effective at expanding the orbits of DM particles near the halo centre, unbinding a fraction of these particles and eventually leading to the formation of a core, as proposed originally by Navarro et al. (1996a).

In both APOSTLE and AURIGA, $n_{\rm sf} = \mathcal{O}(0.1)\,{\rm cm}^{-3}$. By contrast, in the works of Governato et al. (2010, 2012); Di Cintio et al. (2014); Oñorbe et al. (2015); Fitts et al. (2017); Macciò et al. (2017) – where the formation of cores in dwarf galaxies haloes has been reported – the typical values of $n_{\rm sf}$ range from 10-1000 cm$^{-3}$,

---

[5] This calculation assumes a feedback event that occurs in a single, extended burst. Garrison-Kimmel et al. (2013) have argued that a single explosive event is typically more effective than short, repeated bursts (totalling to the same overall outflow mass) at *reducing* the central densities of DM haloes; on the other hand, multiple cycles of outflows are more effective at producing *shallower* density slopes.
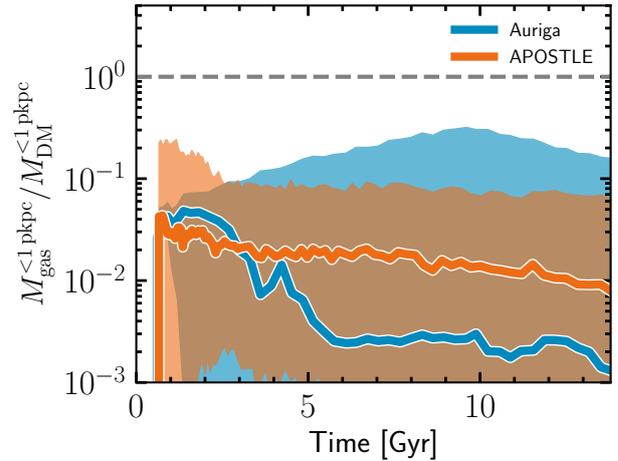


**Figure 9.** Evolution of the ratio of total gas mass to mass in dark matter within the central one physical kiloparsec of isolated dwarfs in the AURIGA (blue) and APOSTLE (orange) simulations. The thick solid lines show the median ratios, while the shaded regions encompass the 10$^{\rm th}$ and 90$^{\rm th}$ percentiles.

that is between 100 to 10,000 times larger than the value adopted in APOSTLE and AURIGA. To draw an analogy with the Navarro et al. (1996a) mechanism, the gravitational potential of the gas in these simulations is allowed to build up to much larger values than in our simulations, with the result that the eventual episodes of feedback from star formation generate gas motions that are more effective at perturbing the orbits of neighbouring DM particles. The absence of cores in APOSTLE and AURIGA is therefore consistent with the predictions of Governato et al. (2010) who showed that a low threshold density $\mathcal{O}(0.1)\,{\rm cm}^{-3}$ (as we have adopted in the present work) is ineffective as forming a core; a value closer to $\mathcal{O}(100)\,{\rm cm}^{-3}$ is required for gas to become concentrated enough to dominate the gravitational potential near the centre.

A consequence of the relatively low threshold for star formation adopted in our simulations is that gas is converted into stars before it is allowed to become gravitationally dominant over the DM. This is demonstrated explicitly in Fig. 9, which shows the evolution with time of the ratio of the mass in gas to the mass in DM within one physical kiloparsec for dwarfs in APOSTLE and AURIGA. The solid lines represent the median ratios over the age of the Universe, while the shaded regions encompass the 10$^{\rm th}$-90$^{\rm th}$ percentiles of the population. This figure shows that total gas mass (and, by extension, gas potential) is always gravitationally subdominant to the DM for all simulated dwarfs. Any fluctuations in the potential that may be induced by gas motions following a feedback event are therefore ineffective at perturbing the potential of the DM particles over the same physical scale, and these systems remain DM-dominated at all times. A systematic demonstration of the effect of varying $n_{\rm sf}$ in simulations similar to APOSTLE has been presented by Benitez-Llambay et al. (2018).

It is important to stress that, in this picture, the entire history of the gas content in dwarfs is relevant, rather than simply how much there is at present day. For example, while the dwarfs that are claimed to have cores may be DM-dominated today, for the core to have formed in the first place the gas content within the inferred core size must have been gravitationally-dominant over the DM. After this gas is eventually expelled by supernovae (potentially forming a core through induced fluctuations in the local potential), it need not return. In principle, therefore, it is possible for

dwarfs that are DM-dominated at present to exhibit cores; considering the entire history of the gas content of these galaxies, which is presently inaccessible in the data, is key.

Finally, it is worth highlighting that there is still considerable debate as to how prevalent cores are in observed dwarfs. As we have discussed previously, there are a number of systematic effects in the techniques used to infer DM density profiles from observational data. For example, Read et al. (2016), Oman et al. (2017) and Pineda et al. (2017) have emphasised the importance of accounting for the presence of thick H I disks and non-circular motions of gas when measuring H I rotation curves. In their mock 'observations' of galaxies from the APOSTLE project Oman et al. (2017) find that viewing these galaxies from different lines-of-sight results in a diverse set of rotation curves *for the same galaxy*. In some cases, particular orientations result in a severe underestimate of the circular velocity in the inner halo, producing a 'core-like' rotation curve when, in fact, the 3D DM density distribution in the simulation has a cusp.

The spatial distribution of stellar populations with kinematically distinct metallicity components in some dwarf galaxies has also been used to infer the mass profile of the surrounding DM halo (e.g. Battaglia et al. 2008; Amorisco & Evans 2012; Strigari et al. 2014). Using this technique, Walker & Peñarrubia (2011) inferred the existence of cores in both the Sculptor and Fornax dwarf spheroidal galaxies. However, as shown recently by Genina et al. (2018), using galaxies extracted from APOSTLE, even this method is sensitive to the viewing angle used to measure the kinematics of these metallicity populations; in particular, the assumption of spherical symmetry can mistakenly lead to the inference of a core when there is actually a cusp.

# 5 CONCLUSIONS

We have carried out a detailed investigation of the dark matter (DM) density profiles of isolated dwarf galaxy haloes in the high-resolution APOSTLE and AURIGA cosmological, hydrodynamical simulations. We have focused specifically on their inner profiles in the context of claims that the presence of cores inferred from the rotation curves of some observed dwarf galaxies represents a short-coming of the popular cold dark matter (CDM) paradigm, wherein collisionless DM-only simulations universally predict cuspy density profiles (Navarro et al. 1996b, 1997).

Some recent simulations (e.g. Governato et al. 2012; Pontzen & Governato 2012; Teyssier et al. 2013; Di Cintio et al. 2014; Brooks & Zolotov 2014; Chan et al. 2015; Oñorbe et al. 2015; Trujillo-Gomez et al. 2015; Fitts et al. 2017; Macciò et al. 2017) have shown that cores in the central parts of CDM halos can form as a result of energetic baryon effects, specifically the repeated injection of supernova energy (following violent episodes of star formation) into the surrounding gas, the resulting outflows of which cause DM particle orbits near the halo centre to move out leading to a new equilibrium system with a central core.

By contrast, the haloes of dwarf galaxies in the APOSTLE (Fattahi et al. 2016b; Sawala et al. 2016) and AURIGA (Grand et al. 2017) simulations have central cusps, not cores. To investigate the differences with the simulations that do produce cores, we selected isolated dwarfs in APOSTLE and AURIGA spanning the mass range $10^9 < M_{\rm DM}/{\rm M_\odot} < 5 \times 10^{10}$. The APOSTLE project simulates the formation of the Local Group and its immediate environment, while the AURIGA project consists of re-simulations of isolated Milky Way-like galaxies. The two sets of simulations differ in their nu-

merical setups: APOSTLE was run with a modified version of the TreeSPH code, P-GADGET-3, while AURIGA was run with the moving mesh code, AREPO. Very similar galaxy formation models to those in APOSTLE and AURIGA have been employed in the larger scale, cosmological simulations of the EAGLE (Schaye et al. 2015) and ILLUSTRIS (Vogelsberger et al. 2014) projects, respectively. These show that these galaxy formation models lead to *galaxy populations* which resemble real galaxy populations in many important properties as a function of time.

Our main conclusions from the current study are:

(i) The size-mass relation of dwarf galaxies in APOSTLE and AURIGA exhibits a similar trend to the data for dwarfs in the Local Group, albeit with a tighter scatter than what is observed (Fig. 1). For all simulated galaxies with stellar mass $M_\star > 10^7 {\rm M_\odot}$, the stellar half-mass radius, $r^\star_{1/2} > 600$ pc; this is nearly two times larger than the nominal resolution limit with which we can reliably measure DM profiles from our simulations. Any length scale imposed by the formation of these galaxies in the DM density profile would have been adequately resolved in both APOSTLE and AURIGA.

(ii) Irrespective of the amount of stellar mass formed within a dwarf galaxy halo, neither APOSTLE nor AURIGA show any evidence of core formation. In fact, as shown in Figs. 2 and 3, the shallowest inner slope attained by the DM density profile of dwarfs in either simulation is $\approx -0.8$, far from the slope of 0 corresponding to a constant density core.

(iii) We find no evidence of any correlation between the evolution of the inner slope of the DM density profile and the star formation rate (SFR) in the APOSTLE or AURIGA dwarf galaxies (Fig. 4); in fact, the evolution of the inner slope is consistent with the natural evolution of the inner slope of the corresponding haloes in DM-only simulations.

(iv) Our simulated dwarfs also show no correlation between the efficiency of star formation, as measured by $M_\star/M_{\rm Tot}$ (where $M_{\rm Tot}$ is the total mass including DM, gas and stars), and the change of the inner slope of the DM density profile in the hydrodynamics simulations compared to the DM-only cases (Fig. 6). While the scatter in this relation is large, the overall trend is consistent with zero.

(v) The star formation histories (SFHs) of a selection of dwarf galaxies extracted from AURIGA and APOSTLE (in particular) are bursty (Fig. 7) even when smoothed over 100 and 200 Myr intervals (timescales comparable to the typical dynamical time for $10^{10} {\rm M_\odot}$ dwarfs at a radius of 1 kpc). The average SFRs for these dwarfs can also be quite high, as large as $\sim 3 \times 10^{-2} {\rm M_\odot} \, {\rm yr}^{-1}$ in some cases.

(vi) While the SFHs of dwarfs in APOSTLE are quite bursty and those in AURIGA less so, dwarfs in both sets of simulations show a similar diversity in SFHs when compared to the data for the real Local Group dwarfs (Fig. 8). In both sets of simulations we find examples of dwarfs that range from early to late forming, and several that show sustained growth of stellar mass throughout their lifetime.

(vii) The fact that density cores are not generated in these simulations, despite the prevalence of bursty SFHs and the availability, in principle, of enough energy from supernovae feedback, demonstrates that these two conditions are, by themselves, *insufficient* for core formation.

One possible explanation for the absence of cores is that our simulations adopt a relatively low gas density threshold for converting gas into stars which prevents the gas from becoming gravitationally dominant on kiloparsec scales (Fig. 9). However, given the subgrid models employed in the simulations, this threshold is

required to achieve a good match to the broad population of galaxies. Recent work by Read et al. (2018) suggests a preference for DM cores in dwarfs that are gas-rich and highly star forming, compared to a propensity for cusps in gas-poor, inactive dwarfs. These findings perhaps indicate the importance for large concentrations of gas over some scale for core formation to be efficient, for example, the massive gaseous clumps that e.g. El-Zant et al. (2001) and Nipoti & Binney (2015) argue can scatter DM particles away from the centre.

If the presence of density cores at the centres of dwarf galaxies is eventually established conclusively, this will require an explanation. One possibility is that the dark matter is more complex than simple CDM. Another possibility is that the sort of baryon effects that we have discussed in this paper do, indeed, operate in nature. It remains to be seen, however, whether a subgrid model can be constructed which leads to the formation of cores in dwarf galaxies while preserving the remarkable successes of the EAGLE and ILLUSTRIS subgrid models in matching properties of the galaxy population across cosmic time.

## REFERENCES

Amorisco N. C., Evans N. W., 2012, MNRAS, 419, 184
Anderhalden D., Diemand J., 2013, J. Cosmology Astropart. Phys., 4, 009
Angulo R. E., Hahn O., Ludlow A. D., Bonoli S., 2017, MNRAS, 471, 4687
Battaglia G., Helmi A., Tolstoy E., Irwin M., Hill V., Jablonka P., 2008, ApJ, 681, L13
Benitez-Llambay A., Frenk C. S., Ludlow A. D., Navarro J. F., 2018, arXiv e-prints,
Bode P., Ostriker J. P., Turok N., 2001, ApJ, 556, 93
Bond J. R., Szalay A. S., 1983, ApJ, 274, 443
Booth C. M., Schaye J., 2009, MNRAS, 398, 53
Bose S., Hellwing W. A., Frenk C. S., Jenkins A., Lovell M. R., Helly J. C., Li B., 2016, MNRAS, 455, 318
Bozek B., Boylan-Kolchin M., Horiuchi S., Garrison-Kimmel S., Abazajian K., Bullock J. S., 2016, MNRAS, 459, 1489
Brooks A. M., Zolotov A., 2014, ApJ, 786, 87
Burkert A., 1995, ApJ, 447, L25
Campbell D. J. R., et al., 2017, MNRAS, 469, 2335
Chan T. K., Kereš D., Oñorbe J., Hopkins P. F., Muratov A. L., Faucher-Giguère C.-A., Quataert E., 2015, MNRAS, 454, 2981
Cole S., Lacey C. G., Baugh C. M., Frenk C. S., 2000, MNRAS, 319, 168
Colín P., Avila-Reese V., Valenzuela O., 2000, ApJ, 542, 622
Crain R. A., et al., 2015, MNRAS, 450, 1937
Dalla Vecchia C., Schaye J., 2012, MNRAS, 426, 140
Davis M., Efstathiou G., Frenk C. S., White S. D. M., 1985, ApJ, 292, 371
Dekel A., Silk J., 1986, ApJ, 303, 39
Di Cintio A., Brook C. B., Macciò A. V., Stinson G. S., Knebe A., Dutton A. A., Wadsley J., 2014, MNRAS, 437, 415
Duffy A. R., Schaye J., Kay S. T., Dalla Vecchia C., Battye R. A., Booth C. M., 2010, MNRAS, 405, 2161
Dutton A. A., Macciò A. V., Buck T., Dixon K. L., Blank M., Obreja A., 2018, arXiv e-prints, p. arXiv:1811.10625
El-Badry K., Wetzel A. R., Geha M., Quataert E., Hopkins P. F., Kereš D., Chan T. K., Faucher-Giguère C.-A., 2017, ApJ, 835, 193
El-Zant A., Shlosman I., Hoffman Y., 2001, ApJ, 560, 636
El-Zant A. A., Freundlich J., Combes F., 2016, MNRAS, 461, 1745
Fattahi A., Navarro J. F., Sawala T., Frenk C. S., Sales L. V., Oman K., Schaller M., Wang J., 2016a, preprint, (arXiv:1607.06479)
Fattahi A., et al., 2016b, MNRAS, 457, 844
Fattahi A., Navarro J. F., Frenk C. S., Oman K. A., Sawala T., Schaller M., 2018, MNRAS, 476, 3816
Fitts A., et al., 2017, MNRAS, 471, 3547
Flores R. A., Primack J. R., 1994, ApJ, 427, L1
Frenk C. S., White S. D. M., 2012, Annalen der Physik, 524, 507
Garrison-Kimmel S., Rocha M., Boylan-Kolchin M., Bullock J. S., Lally J., 2013, MNRAS, 433, 3539
Genina A., et al., 2018, MNRAS, 474, 1398
Governato F., et al., 2010, Nature, 463, 203
Governato F., et al., 2012, MNRAS, 422, 1231
Grand R. J. J., et al., 2017, MNRAS, 467, 179
Hague P. R., Wilkinson M. I., 2013, MNRAS, 433, 2314
Hernquist L., 1990, ApJ, 356, 359
Hopkins P. F., 2013, MNRAS, 428, 2840
Hopkins P. F., Kereš D., Oñorbe J., Faucher-Giguère C.-A., Quataert E., Murray N., Bullock J. S., 2014, MNRAS, 445, 581
Hopkins P. F., et al., 2018, MNRAS, 480, 800
Ishiyama T., 2014, ApJ, 788, 27
Katz N., Weinberg D. H., Hernquist L., 1996, ApJS, 105, 19
Komatsu E., et al., 2011, ApJS, 192, 18
Kuzio de Naray R., Kaufmann T., 2011, MNRAS, 414, 3617
Laporte C. F. P., Peñarrubia J., 2015, MNRAS, 449, L90
Larson R. B., 1974, MNRAS, 169, 229
Lelli F., McGaugh S. S., Schombert J. M., 2016, AJ, 152, 157
Lovell M. R., Frenk C. S., Eke V. R., Jenkins A., Gao L., Theuns T., 2014, MNRAS, 439, 300
Macciò A. V., Frings J., Buck T., Penzo C., Dutton A. A., Blank M., Obreja A., 2017, MNRAS, 472, 2356
Madau P., Shen S., Governato F., 2014, ApJ, 789, L17
Marinacci F., Pakmor R., Springel V., 2014, MNRAS, 437, 1750
Mashchenko S., Couchman H. M. P., Wadsley J., 2006, Nature, 442, 539
Mashchenko S., Wadsley J., Couchman H. M. P., 2008, Science, 319, 174
McConnachie A. W., 2012, AJ, 144, 4

Moore B., 1994, Nature, 370, 629

Navarro J. F., Eke V. R., Frenk C. S., 1996a, MNRAS, 283, L72

Navarro J. F., Frenk C. S., White S. D. M., 1996b, ApJ, 462, 563

Navarro J. F., Frenk C. S., White S. D. M., 1997, ApJ, 490, 493

Nelson D., et al., 2018, MNRAS, 475, 624

Nipoti C., Binney J., 2015, MNRAS, 446, 1820

Oñorbe J., Boylan-Kolchin M., Bullock J. S., Hopkins P. F., Kereš D., Faucher-Giguère C.-A., Quataert E., Murray N., 2015, MNRAS, 454, 2092

Oh S.-H., et al., 2015, AJ, 149, 180

Okamoto T., Frenk C. S., Jenkins A., Theuns T., 2010, MNRAS, 406, 208

Oman K. A., Marasco A., Navarro J. F., Frenk C. S., Schaye J., Benítez-Llambay A., 2017, preprint, (arXiv:1706.07478)

Pakmor R., Marinacci F., Springel V., 2014, ApJ, 783, L20

Parry O. H., Eke V. R., Frenk C. S., Okamoto T., 2012, MNRAS, 419, 3304

Peñarrubia J., Pontzen A., Walker M. G., Koposov S. E., 2012, ApJ, 759, L42

Pillepich A., et al., 2018a, MNRAS, 473, 4077

Pillepich A., et al., 2018b, MNRAS, 475, 648

Pineda J. C. B., Hayward C. C., Springel V., Mendes de Oliveira C., 2017, MNRAS, 466, 63

Planck Collaboration et al., 2014, A&A, 571, A16

Pontzen A., Governato F., 2012, MNRAS, 421, 3464

Power C., Navarro J. F., Jenkins A., Frenk C. S., White S. D. M., Springel V., Stadel J., Quinn T., 2003, MNRAS, 338, 14

Read J. I., Gilmore G., 2005, MNRAS, 356, 107

Read J. I., Iorio G., Agertz O., Fraternali F., 2016, MNRAS, 462, 3628

Read J. I., Walker M. G., Steger P., 2018, preprint, (arXiv:1808.06634)

Revaz Y., Jablonka P., 2018, A&A, 616, A96

Robertson A., et al., 2018, MNRAS, 476, L20

Rocha M., Peter A. H. G., Bullock J. S., Kaplinghat M., Garrison-Kimmel S., Oñorbe J., Moustakas L. A., 2013, MNRAS, 430, 81

Sawala T., et al., 2016, MNRAS, 457, 1931

Schaller M., et al., 2015a, MNRAS, 451, 1247

Schaller M., Dalla Vecchia C., Schaye J., Bower R. G., Theuns T., Crain R. A., Furlong M., McCarthy I. G., 2015b, MNRAS, 454, 2277

Schaye J., 2004, ApJ, 609, 667

Schaye J., Dalla Vecchia C., 2008, MNRAS, 383, 1210

Schaye J., et al., 2015, MNRAS, 446, 521

Shao S., Gao L., Theuns T., Frenk C. S., 2013, MNRAS, 430, 2346

Simpson C. M., Grand R. J. J., Gómez F. A., Marinacci F., Pakmor R., Springel V., Campbell D. J. R., Frenk C. S., 2018, MNRAS, 478, 548

Skillman E. D., et al., 2014, ApJ, 786, 44

Somerville R. S., Primack J. R., 1999, MNRAS, 310, 1087

Sparre M., Hayward C. C., Feldmann R., Faucher-Giguère C.-A., Muratov A. L., Kereš D., Hopkins P. F., 2017, MNRAS, 466, 88

Springel V., 2005, MNRAS, 364, 1105

Springel V., 2010, MNRAS, 401, 791

Springel V., White S. D. M., Tormen G., Kauffmann G., 2001, MNRAS, 328, 726

Springel V., et al., 2008, MNRAS, 391, 1685

Strigari L. E., Frenk C. S., White S. D. M., 2014, preprint, (arXiv:1406.6079)

Teyssier R., Pontzen A., Dubois Y., Read J. I., 2013, MNRAS, 429, 3068

Tollet E., et al., 2016, MNRAS, 456, 3542

Trayford J. W., et al., 2017, MNRAS, 470, 771

Trujillo-Gomez S., Klypin A., Colín P., Ceverino D., Arraki K. S., Primack J., 2015, MNRAS, 446, 1140

Villaescusa-Navarro F., Dalal N., 2011, J. Cosmology Astropart. Phys., 3, 024

Vogelsberger M., Zavala J., Loeb A., 2012, MNRAS, 423, 3740

Vogelsberger M., Genel S., Sijacki D., Torrey P., Springel V., Hernquist L., 2013, MNRAS, 436, 3031

Vogelsberger M., et al., 2014, MNRAS, 444, 1518

Walker M. G., Peñarrubia J., 2011, ApJ, 742, 20

Wechsler R. H., Bullock J. S., Primack J. R., Kravtsov A. V., Dekel A., 2002, ApJ, 568, 52

White S. D. M., Frenk C. S., 1991, ApJ, 379, 52

Wiersma R. P. C., Schaye J., Smith B. D., 2009a, MNRAS, 393, 99

Wiersma R. P. C., Schaye J., Theuns T., Dalla Vecchia C., Tornatore L., 2009b, MNRAS, 399, 574

Zavala J., Vogelsberger M., Walker M. G., 2013, MNRAS, 431, L20

de Blok W. J. G., McGaugh S. S., Rubin V. C., 2001, AJ, 122, 2396